Brain Total Creatine Differs Between Primary Progressive Aphasia (PPA) Subtypes and Correlates with Disease Severity

Kathleen E. Hupfeld[a,b], Helge J. Zöllner[a,b], Georg Oeltzschner[a,b], Hayden W. Hyatt[c], Olivia Herrmann[d], Jessica Gallegos[d], Steve C. N. Hui[a,b], Ashley D. Harris[e,f], Richard A. E. Edden[a,b], and Kyrana Tsapkini[d,g*]

[a] Russell H. Morgan Department of Radiology and Radiological Science, Johns Hopkins University School of Medicine, Baltimore, MD, USA

[b] F. M. Kirby Research Center for Functional Brain Imaging, Kennedy Krieger Institute, Baltimore, MD, USA

[c] Department of Physiology, Johns Hopkins University School of Medicine, Baltimore, MD, USA

[d] Department of Neurology, Johns Hopkins University School of Medicine, Baltimore, MD, USA

[e] Hotchkiss Brain Institute, University of Calgary, Calgary, Alberta, Canada

[f] Alberta Children's Hospital Research Institute, University of Calgary, Calgary, Alberta, Canada

[g] Department of Cognitive Science, Johns Hopkins University, Baltimore, MD, USA

Corresponding Author: Kyrana Tsapkini, PhD
Departments of Neurology and Cognitive Science
Johns Hopkins University
Phipps 488, 600 N Wolfe Street
Baltimore, MD 21287
Email: tsapkini@jhmi.edu

Running Title: BRAIN CREATINE IN PRIMARY PROGRESSIVE APHASIA

Abstract

Background: Primary progressive aphasia (PPA) is a debilitating neurodegenerative disease that primarily impairs language function. It is comprised of three subtypes with varied clinical presentation and cortical atrophy patterns: logopenic variant (lvPPA), non-fluent variant (nfvPPA), and semantic variant (svPPA). No prior work has examined differences in brain chemistry between the PPA subtypes, or associations of brain chemistry with symptom severity.

Methods: We collected magnetic resonance spectroscopy (MRS) data in the left inferior frontal gyrus (IFG, a main language production region) and the right sensorimotor cortex (SMC) from 61 PPA patients. We analyzed tissue-corrected metabolite levels to account for the effects of cortical atrophy and other tissue-specific properties. We aimed to: 1) characterize differences between PPA subtypes for 5 brain metabolites: total N-acetylaspartate (tNAA), total choline (tCho), total creatine (tCr), glutamate+glutamine (Glx), and gamma-aminobutyric acid (GABA); and 2) test for associations between these neurometabolites and PPA symptom severity.

Results: tCr levels differed by PPA subtype across both the left IFG and right SMC. In both regions, tCr levels were lowest among lvPPA patients and highest among svPPA patients. Moreover, across the whole cohort, higher tCr and lower Glx levels in the left IFG correlated with greater disease severity.

Conclusions: Given that tCr is involved in brain energy metabolism and homeostasis, our results indicate that svPPA pathology might involve changes in specific cellular energy processes. Moreover, our finding that higher tCr was associated with worse PPA symptom severity suggests that perturbations to cellular energy homeostasis in cortical language areas may contribute to PPA symptoms. In addition, reduced cortical excitatory capacity (i.e., lower Glx) in brain areas related to language processing may also contribute to PPA symptoms. Together, these findings suggest that tCr could serve as a biomarker to differentiate between PPA subtypes, and that both tCr and Glx might have utility for better understanding PPA disease mechanisms and tracking disease progression.

Trial registration: ClinicalTrials.gov (NCT02606422). Registered 11 November 2015 - Retrospectively registered, https://clinicaltrials.gov/ct2/show/NCT02606422?term=NCT02606422&draw=2&rank=1

Keywords: Primary Progressive Aphasia (PPA), creatine (tCr), glutamate+glutamine (Glx), magnetic resonance spectroscopy (MRS), Point RESolved Spectroscopy (PRESS)

1. Background

Primary progressive aphasia (PPA) is a devastating neurodegenerative condition characterized by prominent declines in language function (1,2). Symptoms usually begin in middle age (around 40-60 years), worsen over time, and may later extend to other cognitive domains (1–3). PPA thus considerably impacts quality of life, in addition to shortening life expectancy; average life expectancy after PPA diagnosis is only about 3-12 years (4). Critically, aside from some symptom improvement with behavioral therapy (5) or neuromodulation (6,7), there remain no disease-modifying treatments for PPA. Therefore, it is becoming increasingly imperative to improve scientific understanding of PPA pathology to identify biomarkers of disease progression as well as potential therapeutic targets.

Consistent with their language symptoms, those with PPA typically display cortical atrophy in the left hemisphere, particularly in brain regions related to language function (8). However, PPA is a heterogeneous disorder associated with both varied symptoms and varied pathology. As such, expert consensus has divided PPA into three subtypes (1) (along with mixed or unclassified cases): 1) logopenic variant PPA (lvPPA) is characterized by deficits in word retrieval (i.e., producing the intended word) and difficulty repeating words and sentences; 2) non-fluent variant PPA (nfvPPA) is characterized by deficits in grammar and speech production and slow, effortful, and distorted (apraxic) speech, but preserved word comprehension and naming; and 3) semantic variant PPA (svPPA) is characterized by severe deficits in single-word comprehension and naming, but preserved grammar and fluency (i.e., these individuals tend to produce “empty” speech).

These three subtypes have been linked to different cortical atrophy patterns and different pathology. Atrophy is most prominent in the left posterior temporal and inferior parietal lobes in lvPPA, left posterior frontal and fronto-insular cortex in nfvPPA, and anterior temporal lobes (left dominant but usually bilateral) in svPPA (1). lvPPA is most often associated with Alzheimer’s disease (AD) pathology (e.g., PET-PIB positivity, decreased Aβ42, and elevated tau in the

99 cerebrospinal fluid) (9,10), nfvPPA is most often associated with tau-positive pathology
100 (9,11,12), and svPPA is most often associated with ubiquitin/TDP43-positive frontotemporal
101 lobar degeneration (3,9,13–15). However, there is not a direct correspondence between atrophy
102 or pathology and PPA subtype; thus, further work is warranted to better understand how
103 disease mechanisms might differ between the PPA subtypes.

104 Magnetic resonance spectroscopy (MRS) permits measurement of brain chemicals *in*
105 *vivo* in humans using an MRI scanner and thus can provide insight into potential disease
106 mechanisms and drug targets, distinct from conclusions that can be drawn from the atrophy and
107 pathology measurements discussed above. Standard MRS acquisitions, including short-echo
108 time (TE) Point RESolved Spectroscopy (PRESS), measure metabolites including total *N*-acetyl
109 aspartate (tNAA), total choline (tCho), total creatine (tCr), and glutamate+glutamine (Glx) (16).
110 tNAA, a composite measure of NAA and NAAG (N-acetylaspartylglutamate), is a neuronal
111 marker, suggested as an indicator of neuronal density and integrity (17). tCho, the composite of
112 phospholipid precursors phosphocholine (PCh) and glycerophosphocholine (GPC), can reflect
113 changes in membrane turnover or cell density (18). Creatine and phosphocreatine (reported in
114 combination as tCr) are involved in brain energy metabolism and homeostasis (17). Glx is a
115 combination of two signals: glutamate (i.e., the principal excitatory neurotransmitter in the
116 central nervous system (CNS)) and glutamine (i.e., a precursor for glutamate). *J*-difference
117 editing of the spectrum using e.g., MEscher–GArwood Point RESolved Spectroscopy (MEGA-
118 PRESS) (19–21) allows us to quantify additional metabolites with coupled spin systems and
119 overlapped signals. These include the primary inhibitory neurotransmitter within the CNS,
120 gamma-aminobutyric acid (GABA).

121 A majority of studies suggest that brain tNAA, Glx (or glutamate), and GABA levels
122 decrease with normal aging (18,22–24), and are decreased in mild cognitive impairment (MCI)
123 (25,26) and AD (27–30) compared with normal aging. Both tCho and tCr either increase or show
124 no change with normal aging (18,22,24), and are either elevated (31,32) or not different (29,32)

in MCI and AD compared with normal aging. Functionally, lower MRS-measured tNAA, Glx (or glutamate), and GABA, and higher tCho, have each been associated with poorer cognitive performance in normal aging (33–37), MCI (25,38–40), AD (39), and frontotemporal lobar degeneration patients (41). Taken together, it is plausible that these metabolites might differ between the three PPA subtypes and associate with metrics of disease severity.

We previously identified GABA decreases in the left inferior frontal gyrus (IFG) following transcranial direct current stimulation (tDCS) combined with language therapy in PPA patients (42). However, the sample size included in this prior work (*n* = 22) was not sufficient to stratify metabolite level differences by the three PPA subtypes. Therefore, the objectives of the present study included: 1) to characterize differences in brain metabolite levels between the three PPA subtypes; and 2) to examine relationships between brain metabolite levels and PPA symptom severity, as indicated by the FrontoTemporal Dementia Clinical Dementia Rating Scale (FTD-CDR, a measure of overall disease severity, including language function, memory, attention, and independence, with scores ranging from 0 (no impairment) to 24 (severe impairment) (43)).

2. Methods

2.1 Participants

Prior to study enrollment, all patients were evaluated using neurological examination, cognitive and language testing, and neuroimaging. All patients enrolled in the study were diagnosed with PPA using current consensus criteria (1); diagnoses were confirmed by expert clinicians. Additional inclusion criteria included: at least a 12th grade education, right-handedness, and English as a first language. Participants were excluded if: they were over 90 years of age, were not pre-morbidly proficient spellers, had progressed to advanced stages of PPA or other dementia, had any diagnosed comorbid neurologic conditions (e.g., stroke, psychiatric, or developmental disorder), or if they had any contraindications for MRI scanning. The Johns Hopkins University Institutional Review Board (#NA_00071337) approved all study

procedures, and the trial was registered on ClinicalTrials.gov (NCT02606422). All participants scored >0 on the FTD-CDR scale, indicating at least some level of impairment to daily functioning.

2.2 MRS Acquisition

All MRS data were collected using the same 3.0 Tesla Philips Achieva MRI scanner using a 32-channel head coil. For voxel positioning and tissue segmentation, we collected a whole-brain T_1-weighted structural MRI scan, using the following parameters: magnetization-prepared rapid gradient-echo (MPRAGE) sequence, TR/TE = 8 ms/3.75 ms, flip angle = 8°, slice thickness = 1.0 mm, 150 slices, voxel size = 1 mm^3 isotropic voxels. Next, we acquired metabolite spectra from two 30 x 30 x 30 mm^3 voxels (Fig. 1) using both short-TE PRESS and MEGA-PRESS sequences. We positioned the left IFG voxel using the anatomical landmarks of the lateral ventricles and insula. We positioned the right SMC voxel by centering the voxel on the hand knob in the precentral gyrus. Both voxels were carefully shifted and rotated to avoid the edge of the brain and ventricles as much as possible to avoid lipid contamination and partial-volume effects.

To measure tNAA, tCho, tCr, and Glx, we used a standard short-TE PRESS acquisition with the following parameters: TR/TE = 2000 ms/32 ms; 48 averages sampled at 2000 Hz with 2048 points; and water suppression using the VAPOR method (44). To resolve GABA, we used MEGA-PRESS (20,21) with the following parameters: TR/TE = 2000 ms/68 ms; 14-ms editing pulses at 1.9 ppm and 7.46 ppm, alternating every 2 averages; 320 averages in total; and VAPOR water suppression (44). MEGA-PRESS editing schemes for the detection of GABA co-edits homocarnosine and macromolecular signals (45); therefore, as is standard practice, we refer to the edited 3 ppm GABA signal as GABA+ in the remainder of the manuscript. For both the short-TE PRESS and MEGA-PRESS acquisitions, we also collected 8 water reference spectra without water suppression or pre-inversion, for later use in eddy current correction and metabolite quantification.

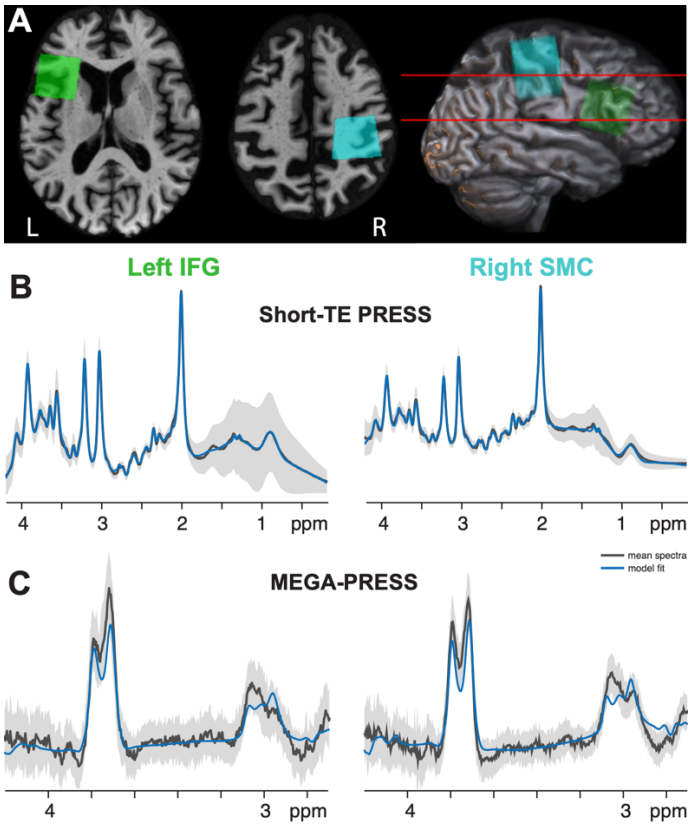

Fig 1. Voxel Placement and Spectra. (A) *In vivo* MR spectra were acquired from the left inferior frontal gyrus (IFG) and right sensorimotor cortex (SMC); here we depict the placement of both voxels (IFG in green, SMC in blue) for a single exemplar participant overlaid onto their skull-stripped structural image to protect patient privacy. The rendered structural image is shown as semi-transparent, in order to depict voxel placement within the brain. **(B-C)** Average short-TE PRESS and GABA-edited MEGA-PRESS spectra (black), 95% confidence interval (gray shading) and model fits (blue) for all participants for both voxels. The PRESS spectra are shown from 0.2-4.2 ppm. The MEGA-PRESS spectra are shown from 2.7-4.2 ppm.

2.3 MRS Data Processing

MRS data were analyzed using the open-source analysis toolbox Osprey (v2.0.0; https://github.com/schorschinho/osprey/) (46) within MATLAB R2021b. The analysis procedures followed consensus-recommended processing guidelines for PRESS and MEGA-PRESS data (19,47) and match those applied in our previous work (48,49). Briefly, for the short-TE PRESS data, analysis steps included: loading the vendor-native raw data (which had already been coil-combined, eddy-current-corrected, and averaged on the scanner at the time of data collection), removing the residual water signal using a Hankel singular value decomposition (HSVD) filter (50), and modeling the metabolite peaks as described in detail in (46,48) using a custom basis set generated by our new MRSCloud tool (https://braingps.anatomyworks.org/mrs-cloud; (51)).

196 The basis set was generated using PRESS localization at TE = 32 ms with the Philips-specific
197 sequence timing and real RF pulse waveforms, and consisted of simulations of 32 metabolites
198 including NAA and NAAG (=tNAA), Cr and PCr (=tCr), GPC and PCh (=tCho), Glu and Gln
199 (=Glx), and GABA (which are of interest in this study), as well as 23 other low-concentration
200 metabolites. We then created a binary mask of the two MRS voxels in subject space, co-
201 registered these masks to each participant's T_1-weighted structural scan, and segmented the
202 structural scans using SPM12 (52), and quantified metabolite levels with respect to the
203 unsuppressed water scan. These tissue volume fractions in the MRS voxels were used for full
204 tissue- and relaxation-corrected metabolite quantification (see below).

205 For the GABA-edited MEGA-PRESS data additional, standardized analysis steps in
206 Osprey included: eddy-current correction based on the water reference (53), robust spectral
207 registration (54) to separately align the individual transients within each sub-spectrum, and final
208 alignment of the averaged sub-spectra by minimizing the choline peak in the difference
209 spectrum before generating the final GABA-edited difference spectrum. The co-edited
210 macromolecules (MMs) at 3 ppm were modelled with the "1to1GABA" model, which uses one
211 composite GABA + MM basis function (i.e., the sum of the GABA and MM_{3co} basis functions,
212 with a fixed 1:1 amplitude ratio); this model assumes 50% of the 3-ppm signal in the GABA-
213 edited difference spectrum can be attributed to co-edited MMs (49,55). As is standard for 3 T
214 GABA-edited MEGA-PRESS data, we considered the composite edited 3-ppm signal, i.e.,
215 "GABA+" (GABA+MM) values in our statistical analyses.

216 Finally, we corrected all metabolite estimates in order to assess metabolite levels only in
217 the tissue present in the voxel, which is particularly relevant for aging and neurodegenerative
218 disease populations who may have substantial cortical atrophy (56). We applied tissue and
219 relaxation correction to the short-TE PRESS values; this adjusts metabolite estimates to
220 account for atrophy and heterogeneous tissue composition within the voxels, using literature
221 values (57) to account for differences in water visibility and relaxation times between tissue

222 types (58,59). Similarly, to account for the effects of atrophy and tissue-specific water visibility
223 and relaxation, (and assuming that GABA+ levels in gray matter are twice that in white matter),
224 we applied the "alpha" correction to all GABA+ values (59). For further details, see Appendix A,
225 in which we list all consensus-recommended parameters regarding our MRS data acquisition,
226 processing, and quality (60).

227 **2.4 Statistical Analyses**

228 We conducted all statistical analyses using R 4.0.0 (61) within RStudio (62). First, we
229 used one-way ANOVAs (or Kruskal-Wallis non-parametric tests if the ANOVA assumptions of
230 normality and heteroskedasticity were not met) to test for group differences in demographic
231 variables and symptom severity between the three subtypes. Next, we used linear mixed
232 models (*lme*, (63)) to examine whether metabolite levels differed by PPA subtype or brain
233 region. In the final model, we entered the metabolite level as the outcome variable, PPA
234 subtype and voxel (i.e., IFG or SMC) as predictors, and included a random intercept for each
235 subject (similar to our previous work, (64)). Including the PPA subtype*voxel interaction term or
236 a random slope for each subject did not improve model fit (likelihood ratio test $p > 0.05$), so
237 these terms were omitted from the final statistical models. Each final model satisfied the linear
238 mixed model assumptions of homogeneity of variances and normality of residuals. We used this
239 same linear mixed model approach to test for PPA subtype and brain region differences in bulk
240 tissue composition (i.e., voxel gray matter, white matter, and cerebrospinal fluid fractions).

241 Lastly, we applied a linear model to test for relationships between brain metabolite levels
242 and PPA symptom severity (i.e., FTD-CDR scores). Given the subgroup sizes and the missing
243 MRS and FTD-CDR data (see Table B1), we conducted this analysis across the whole cohort
244 instead of stratified by PPA subtype. In addition, given the amount of missing GABA+ data
245 compared with the other metabolites (Table B1), we did not include GABA+ as a predictor in this
246 metabolite-symptom severity model (though we did test for GABA+ differences between PPA
247 subtypes, as described above). Thus, in the full model, we entered as predictors: the metabolite

levels from both voxels (4 metabolites/voxel), age, sex, and years since diagnosis. We then selected a final model using *bestglm* with cross-validation, delete-d method, and 1,000 replications to produce a final model that retained only the best predictors of FTD-CDR score (65,66). The FTD-CDR scores were not normally distributed (Shapiro test $p < 0.05$), so we reran the same model selection procedure after square root-transforming the FTD-CDR variable, which improved the normality of the data (Shapiro test $p > 0.05$).

3. Results

3.1 Sample Characteristics

The total cohort consisted of 61 PPA patients: 22 nfvPPA, 27 lvPPA, and 12 svPPA. There were no differences in sex, age, time since diagnosis, or symptom severity based on PPA subtype (Table 1). IFG short-TE PRESS data was not collected for 2 participants, IFG MEGA-PRESS data was not collected for 1 participant, and FTD-CDR scores were missing for 7 participants. Table B1 details additional data omissions from statistical analyses; MRS data were excluded if NAA linewidth was greater than 15 Hz (47) or if incorrect pulse sequence parameters were used during acquisition. Group mean spectra (after these exclusions) are presented in Fig. 1, and data quality metrics (i.e., linewidth, SNR, and fit error) are presented in Appendix A.

Table 1. Sample Characteristics

	lvPPA	nfvPPA	svPPA	F or χ^2	*p*	η^2
n	22	27	12	--	--	--
Sex	13 F; 9 M	11 F; 16 M	7 F; 5 M	1.97	0.373	--
Age (years)	65.58 (8.11)	68.65 (6.61)	69.07 (5.16)	1.50	0.231	0.05
Years of education[a,b]	16.48 (1.91)	16.83 (2.44)	16.35 (2.33)	0.23	0.799	0.01
Years since diagnosis[a,c]	3.93 (2.83)	3.81 (2.58)	5.05 (2.91)	0.83	0.442	0.03
FTD-CDR sum score[a,d]	6.55 (5.17)	5.26 (4.17)	7.61 (5.59)	0.87	0.424	0.03

Table 1 Note. For each metric, we report the mean (standard deviation) for each PPA subtype. We also report the results of one-way ANOVAs to characterize differences in each variable between the subtype groups. For sex, we report the number of males (M) and females (F) and the result of a Pearson's chi-square test for differences in the sex distribution within each group. This table includes all available participants; however, statistical analyses of MRS data omitted several additional participants (see Table B1).

[a] In cases where the variable did not meet the one-way ANOVA assumptions of homogeneity of variances between groups, independence of residuals, and/or normality of residuals (indicated by the subscript 'a'), we reran each analysis using the non-parametric Kruskal-Wallis test. In all cases, the non-parametric test did not change the statistical significance of the result.

[b] Years of education was unavailable for 1 lvPPA, 3 nfvPPA, and 2 svPPA patients.

[c] Years since diagnosis was unavailable for 1 lvPPA, 3 nfvPPA, and 1 svPPA patients.

[d] FTD-CDR sum score was unavailable for 4 nfvPPA patients and 3 svPPA patients.

3.2 Differences in Brain Metabolite Levels by PPA Subtype

tCr levels differed by subtype across both voxels; svPPA patients had higher mean tCr compared with lvPPA patients ($p = 0.019$; Fig. 2; Table 2). nfvPPA patients had higher mean tCr levels compared with lvPPA patients, though this difference did not reach statistical significance within the linear mixed effects model ($p = 0.071$; Fig. 2; Table 2). There were no other differences in brain metabolite levels (all $p > 0.05$; Fig. 2; Table 2) or voxel tissue fractions (all $p > 0.05$; Table B3) based on PPA subtype.

3.3 Regional Differences in Brain Metabolites and Voxel Composition

tNAA was lower in the IFG compared with the SMC voxel ($p < 0.001$), while tCho, tCr, and Glx were higher in the IFG compared with the SMC voxel (all $p < 0.001$; Fig. 2; Table 2). GABA+ did not differ by brain region ($p = 0.626$; Fig. 2; Table 2). The IFG compared with the SMC voxel had a higher gray matter ($p < 0.001$) and lower white matter fraction ($p < 0.001$), as well as a greater total tissue fraction (i.e., higher gray matter + white matter fraction; $p = 0.012$; Table B3).

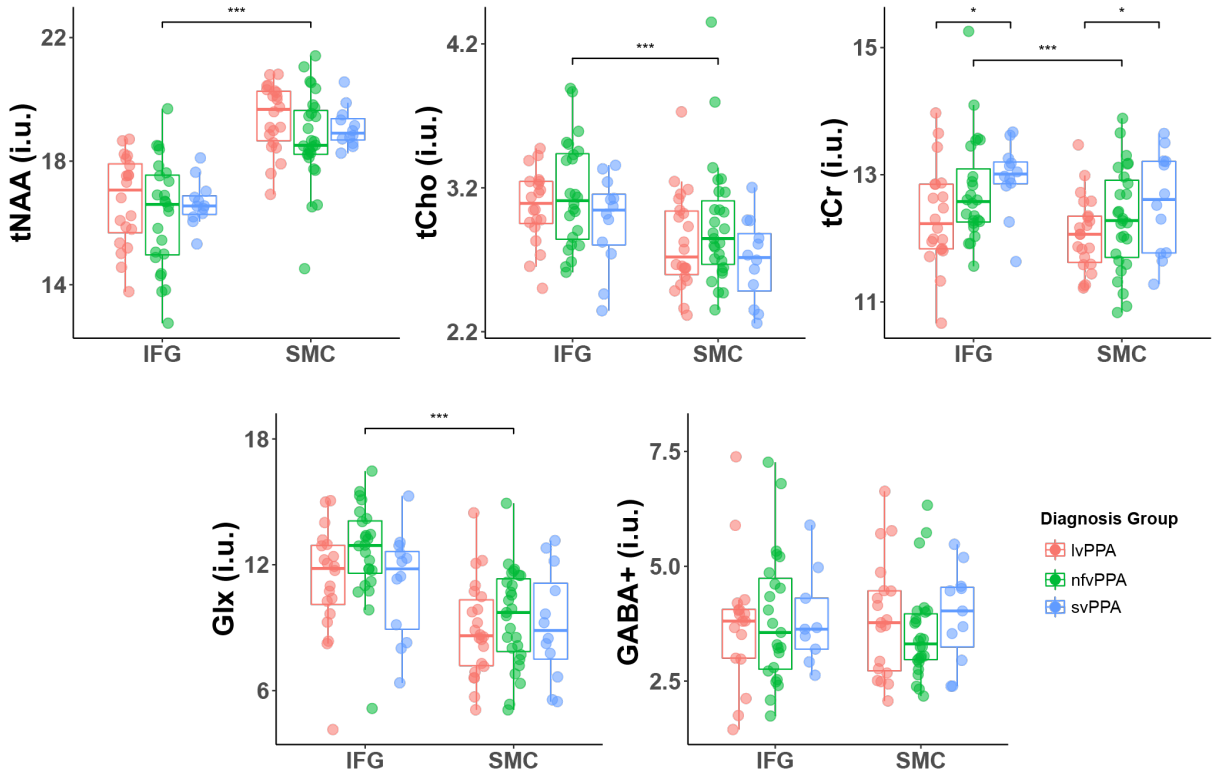

Fig 2. Differences in Metabolites by PPA Subtype and Brain Region. Metabolite levels for the lvPPA (pink), nfvPPA (green), and svPPA (blue) subtypes are shown for the IFG (left) and SMC (right) voxels.
* indicates $p < 0.05$ for the comparison of svPPA tCr levels with lvPPA tCr levels.
*** indicates $p < 0.001$ for the comparison of metabolite values within the SMC versus the IFG.

Table 2. Differences in Metabolites by PPA Subtype and Brain Region

Predictors	Estimates (SE)	CI	t	*p*
tNAA (i.u.)				
Diagnosis *(nfvPPA)*	-0.53 (0.33)	-1.19-0.12	-1.60	0.115
Diagnosis *(svPPA)*	-0.17 (0.41)	-0.98-0.64	-0.41	0.684
Voxel *(SMC)*	2.58 (0.19)	2.20-2.95	13.44	**< 0.001*** **
tCho (i.u.)				
Diagnosis *(nfvPPA)*	0.11 (0.09)	-0.07-0.28	1.22	0.227
Diagnosis *(svPPA)*	-0.12 (0.11)	-0.34-0.09	-1.12	0.269
Voxel *(SMC)*	-0.26 (0.05)	-0.35-(-0.16)	-5.38	**< 0.001*** **
tCr (i.u.)				
Diagnosis *(nfvPPA)*	0.34 (0.18)	-0.02-0.69	1.84	0.071
Diagnosis *(svPPA)*	0.54 (0.23)	0.10-0.99	2.40	**0.019***
Voxel *(SMC)*	-0.40 (0.11)	-0.61-(-0.19)	-3.78	**< 0.001*** **
Glx (i.u.)				
Diagnosis *(nfvPPA)*	0.91 (0.60)	-0.27-2.09	1.51	0.136
Diagnosis *(svPPA)*	0.01 (0.74)	-1.45-1.47	0.01	0.988
Voxel *(SMC)*	-2.58 (0.33)	-3.23-(-1.93)	-7.79	**< 0.001*** **
GABA+ (i.u.)				
Diagnosis *(nfvPPA)*	-0.10 (0.28)	-0.65-0.45	-0.37	0.716
Diagnosis *(svPPA)*	0.10 (0.36)	-0.60-0.80	0.28	0.782
Voxel *(SMC)*	-0.11 (0.23)	-0.57-0.34	-0.49	0.626

Table 2 Note. Here we report the results of a linear mixed effects model testing for PPA subtype and voxel differences in each metabolite. lvPPA and IFG served as the reference groups. For ease of interpretation, in this table we included only the predictors of interest; see Table B2 for all model and fit information. SE = standard error; CI = 95% confidence interval. *$p < 0.05$, ***$p < 0.001$.

3.4 Metabolite Relationships with PPA Symptom Severity

We included all short-TE PRESS metabolite levels from both voxels (i.e., 4 measures/voxel), age, sex, and years since diagnosis in the full statistical model, and only those participants without missing short-TE PRESS or FTD-CDR data (*n* = 49; see Table B1). The final model retained left IFG tCr, left IFG Glx, and years since diagnosis as statistically significant predictors of FTD-CDR score (Table 3). That is, across the whole cohort, worse PPA symptoms (i.e., higher FTD-CDR scores) were associated with higher left IFG tCr levels (partial r = 0.39; *p* = 0.007; Fig. 3A), lower left IFG Glx levels (partial r = -0.36; *p* = 0.012; Fig. 3B), and longer disease duration (partial r = 0.34; *p* = 0.021). Rerunning this model with the square root of FTD-CDR scores as the outcome variable (to meet the normality assumption) returned the same three predictors and did not change the statistical significance of any results.

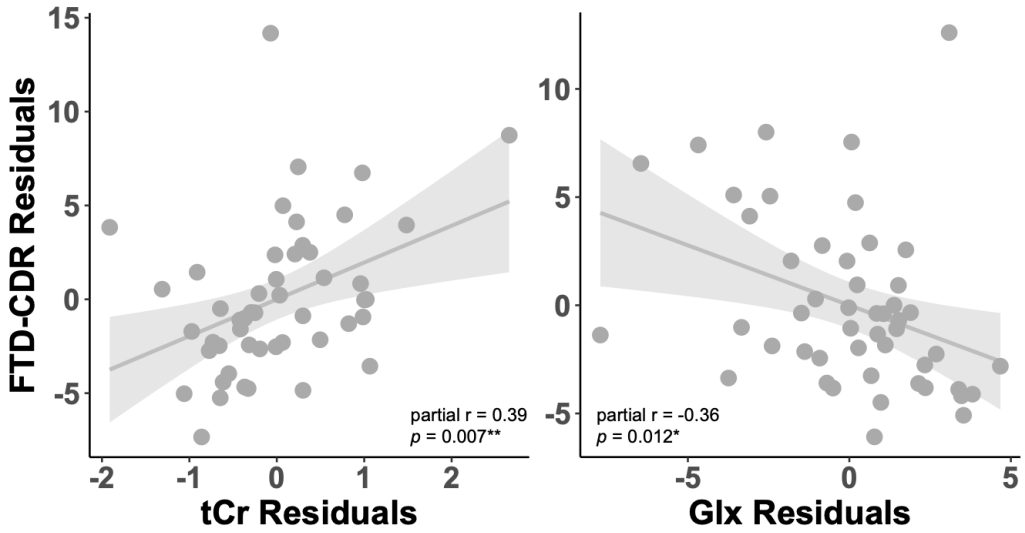

Fig 3. Relationship of IFG tCr and Glx with FTD-CDR Score. This figure depicts the partial correlations of tCr and Glx levels in the left IFG with FTD-CDR scores across all participants (indicated by each gray point). These partial correlations account for the effects of the other predictors included in the final statistical model on the variable of interest (i.e., tCr values are corrected for Glx and years since diagnosis, and Glx values are corrected for tCr and years since diagnosis). Higher FTD-CDR scores indicate worse PPA symptom severity. These plots include *n* = 49 individuals, after exclusion of missing and unusable data (see Table B1).

Table 3. Metabolites Relationships with PPA Symptom Severity

Predictors	Estimates (SE)	CI	t	*p*	R^2 / R^2 Adjusted
(Intercept)	-14.18 (9.19)	-32.69-4.32	-1.54	0.130	
IFG tCr (i.u.)	1.96 (0.69)	0.57-3.35	2.84	**0.007****	
IFG Glx (i.u.)	-0.55 (0.21)	-0.98-(-0.13)	-2.61	**0.012***	
Years since diagnosis	0.48 (0.20)	0.08-0.89	2.39	**0.021***	
					0.34 / 0.29

Table 3 Note. Here we report the results of the final linear model testing for associations between brain metabolite levels and FTD-CDR (i.e., PPA symptom severity) scores. SE = standard error; CI = 95% confidence interval. *$p < 0.05$, **$p < 0.01$.

4. Discussion

This is the first study to investigate brain metabolite differences between PPA subtypes using MRS. Our key findings included, firstly, that tissue-corrected tCr differed by PPA subtype across the left IFG and right SMC; lvPPA patients had the lowest tCr levels, followed by nfvPPA, and svPPA patients with the highest brain tCr levels. Secondly, higher tissue-corrected tCr and lower Glx levels in the left IFG (i.e., a brain region critical for language function) were associated with more severe symptoms as indicated by the FTD-CTR scale (which indexes language function as well as other cognitive and daily living domains (43)). Together, these results suggest that brain tCr may play a role in PPA pathology or progression, particularly for the svPPA subtype, and thus could have utility for differentiating svPPA from other PPA subtypes. Both tCr and Glx might be explored as biomarkers for tracking disease severity and progression.

Those with svPPA had the highest tCr levels across both the left IFG and right SMC. The creatine (Cr)/phosphocreatine (PCr) system is a short-lived energetic system that allows exchange of high-energy phosphate between Cr, adenosine triphosphate (ATP), and adenosine diphosphate (ADP). Creatine kinase, the primary enzyme in the Cr system, reversibly exchanges high-energy phosphate between ATP and Cr (forming PCr) or PCr and ADP (forming ATP). In doing so, the Cr/PCr system simultaneously supplies a high-energy pool capable of rapidly regenerating ATP during high energetic demands, while also dispersing ATP across the cell to connect ATP consumption to the site of energy production (i.e., a bucket-

361 brigade of ATP dispersion (67)). Cr is found in the highest concentrations in tissues with high
362 ATP demand, including muscle and brain tissue (17,68). MRS at 3 T permits measurement of
363 tCr (i.e., the sum of Cr and PCr); tCr is thus reflective of the Cr/PCr system more generally,
364 including PCr anabolism (via Cr synthesis enzymes glycine amidinotransferase (AGAT) and
365 guanidinoacetate methyltransferase (GAMT)), Cr degradation (non-enzymatic conversion to
366 creatinine), and Cr extracellular transport (via Cr transporter, SLC6A8).

367 Previous MRS studies have reported elevated tCr in normal aging (18,22,24,69–72),
368 MCI and AD (31), and other neurological conditions with cognitive symptoms (e.g., HIV-positive
369 patients with neurological symptoms (73,74)). It remains unclear whether this is due to
370 increased Cr and/or PCr synthesis, or decreased clearance of these metabolites from the brain
371 (71). It is hypothesized that elevated brain tCr is related to declines in creatine kinase activity
372 with aging and neurological disease (22,69,70,75–77), possibly due to elevated oxidative stress
373 (67,78). In the present work, it could be that svPPA patients encounter the greatest oxidative
374 stress and resulting perturbation to Cr/PCr cellular energy processes. Future MRS studies that
375 edit for antioxidant levels (e.g., glutathione and ascorbate, (79)) could better elucidate potential
376 contributions of declining antioxidant systems to PPA disease processes.

377 It is also plausible that elevated levels of tCr could be a compensatory mechanism for
378 reduced mitochondrial trafficking in neurons of svPPA individuals. Mitochondrial trafficking
379 refers to the movement of mitochondrial organelles across the cell. Due to the large length of
380 axonal projections in neurons, new mitochondria arising from mitochondrial biogenesis must be
381 delivered from the soma to distal axons (80). Once arrived, mitochondria are anchored in the
382 cell by the protein syntaphilin (SNPH), which abolishes the movement of mitochondria (81).
383 Notably, a recent report showed that SNPH was significantly elevated in a cohort of individuals
384 with TDP43-positive frontotemporal lobar degeneration (82), which is the pathology most
385 associated with the svPPA subtype (1). In this manner, elevated SNPH could result in
386 decreased mitochondrial motility, resulting in a greater need to disperse high-energy phosphate

387 across the cell from sites of production (e.g., mitochondria) to sites of energy consumption (e.g.,
388 neuronal synapses). In this regard, elevated Cr may compensate for an inability to appropriately
389 localize mitochondria across neurons and allow for transport of high-energy phosphate across
390 Cr molecules via creatine kinase. In support of this, neurons lacking appropriate mitochondrial
391 trafficking machinery have markedly reduced ability to form long dendrites; however, this is
392 rescued with Cr supplementation (83). Finally, mitochondrial trafficking has been observed to
393 decrease with older age in animal models (84,85), which may also contribute to reports of
394 elevated brain tCr with aging (18,22,24,69–72). Nonetheless, our understanding of both svPPA
395 pathology and mitochondrial trafficking remain incomplete, and further work is needed to better
396 understand potential mitochondrial trafficking deficiencies and relationships with brain tCr levels.
397 Some authors have suggested that elevated tCr in aging and neurologic disease
398 represent gliosis (69,86,87), as glial cell concentration of tCr is about two to four times that of
399 neurons (88), and prior work has found elevated tCr levels in non-human primates with
400 moderate compared to mild gliosis (87). PPA is associated with a significant accumulation of
401 activated microglia in both gray (89) and white matter (90), particularly in heavily atrophied
402 regions of the language-dominant hemisphere (89,90). Microglia (i.e., the macrophages of the
403 brain) become “activated” in response to neuronal damage, inflammation, and other brain
404 pathology (91,92). This thus fits with our finding of higher tCr levels in the left IFG (i.e., the more
405 affected language cortex in PPA) compared with the right SMC. In addition, activated microglia
406 have been reported to occur close to pathologic insults such as TDP43 inclusions in PPA
407 patients with TDP43-positive pathology (89), i.e., the pathology most associated with svPPA (1).
408 Moreover, it is interesting that tCr levels were the highest in svPPA, as this PPA subtype
409 is typically associated with the most severe behavioral disturbances (93,94) (though we did not
410 find group differences in symptom severity; however, the svPPA group had the most severe
411 average symptom scores). In addition to the potential explanations for elevated tCr levels
412 described above, other prior work has found the most widespread, bilateral cortical atrophy for

svPPA patients (1). Therefore, though the metabolite estimations presented here are corrected for cortical atrophy, greater atrophy in svPPA still suggests that more of the brain is affected by disease processes compared with the other two PPA subtypes. However, there remain very few studies describing brain differences between PPA subtypes; thus, it is difficult to closely compare the present findings with past work.

We found that both higher tCr and lower Glx levels correlated with more severe PPA symptoms, as indicated by the FTD-CDR inventory. This suggests that higher brain tCr and lower brain Glx levels could be (directly or indirectly) related to maladaptive disease processes. These brain-behavior relationships occurred only for the left IFG but not the right SMC. The regional specificity of this association is plausible (and was hypothesized), as the FTD-CDR inventory includes both language and cognitive function sections; the left IFG is involved in language selection and production (e.g., both oral and written naming and spelling) and cognition (e.g., articulatory loop in working memory) (95), while the SMC roles are mostly related to motor execution and sensory processing. Higher tCr levels might indicate disruptions in underlying cellular bioenergetic processes, which could contribute to the development of more severe language and cognitive symptoms in PPA patients; however, such claims warrant further replication in future studies with larger samples, as well as exploration of tCr relationships with additional cognitive metrics.

While we found that elevated brain tCr levels correlated with the most severe PPA symptoms, and others have reported elevated tCr in AD (31), higher brain tCr levels might not be entirely dysfunctional; the relationship between tCr levels and PPA disease processes could be more complex. For instance, oral Cr supplementation has been shown to improve cognitive function in normal adults (96) (though results were variable dependent on cognitive domain, effect sizes were small-moderate, and no large-scale Cr supplementation studies have been conducted in PPA patients). Moreover, multiple prior studies have reported *lower* tCr levels or no difference in tCr levels for normal aging cohorts (18). While these studies used varying

methods (e.g., different MRI scanner field strengths and different brain regions), it remains unclear what other factors might influence brain tCr changes in aging and disease.

Prior work has identified relationships between lower Glx (or glutamate) and poorer cognitive and visuomotor performance in both normal aging (97,98) and neurodegenerative disease (i.e., MCI (25,26) and frontotemporal lobar degeneration (41,99)). Reduced Glx could indicate loss of glutamatergic neurons or disturbances in glutamate and/or glutamine synthesis, which could each reasonably contribute to poorer functional performance. Moreover, as glutamate is a component involved in the synthesis of glutathione (i.e., one of the most abundant brain antioxidants), it could also be that increased brain oxidative stress in response to disease processes would result in greater glutathione production (64,100), and thus lower detectable brain glutamate levels. In our cohort, tCr was not correlated with Glx levels in either the IFG (Pearson r = -0.04; p = 0.782) or SMC (Pearson r = 0.13; p = 0.383), and thus each metabolite may distinctly contribute (directly or indirectly) to PPA disease processes. Further investigation is warranted to better understand the precise mechanisms by which tCr and Glx might associate with PPA symptoms and progression.

We identified differences in brain metabolite levels by PPA subtype only for tCr, but not for the other four investigated metabolites. The metabolite values reported here are corrected for bulk tissue concentrations (58,59); that is, we report metabolite values only within the brain tissue that remains in the voxels, accounting for age-related atrophy of gray and white matter. Therefore, though the three PPA subtypes are associated with differing cortical atrophy patterns (1), our results are not likely explained by group differences in atrophy location and severity. Moreover, as we did not identify group differences in tNAA levels, it is less likely that the tCr group difference is driven by diffuse neuronal loss; instead, we predict that these group differences in tCr are more related to differences in brain energy metabolism, though this hypothesis warrants further investigation in larger cohorts.

There are several limitations to this work. Our cross-sectional approach precluded us from assessing how these metabolite levels may alter prior to PPA onset and with disease progression. Though both age and years since diagnosis did not differ between PPA subtypes, and years since diagnosis was distinct from the relationships between IFG tCr and Glx and symptom severity, it still could be that disease progression rather than subtype more strongly influences brain metabolite levels. PPA is relatively rare and difficult to diagnose (43); thus, we could not compare individuals at the same stage in their disease progression. Brain metabolite levels for one or more subtypes may not differ substantially from normal aging; however, due to the lack of a normal aging control group, we were unable to determine this. There were no differences in the relationship between tCr and symptom severity based on PPA subtype, though all groups trended in the same direction; however, we were likely underpowered to investigate any group differences in this brain-behavior relationship. In addition, there are several inherent limitations to the MRS methods used. Current methods do not allow us to distinguish the contribution of PCr versus Cr to the tCr signal, or the contribution of glutamate versus glutamine to the Glx signal. The tissue corrections applied here are standard for aging cohorts with cortical atrophy (58,59); however, these corrections use literature values (57) for relaxation constants. Changes in water and metabolite relaxation rates with aging and disease could also impact metabolite quantification (101–103), though these were not quantified and thus cannot be incorporated into tissue corrections. Finally, PPA patients often have more difficulty than others remaining still in the scanner, which could have affected spectral quality (though we excluded any participants with NAA linewidth > 15 Hz); moreover, ability to complete an MRI scan precluded us from enrolling any extremely advanced PPA cases in this cohort.

5. Conclusions

We found that brain tCr is different between PPA subtypes (i.e., the highest for svPPA patients). We also found a correlation between both higher left IFG tCr levels and lower left IFG Glx levels and more severe PPA symptoms. tCr could be useful in differentiating between PPA

subtypes, and both tCr and Glx could have utility as markers of PPA symptom severity. However, further work in larger cohorts is needed to better understand the potential roles of tCr and Glx in PPA development and progression.

Ethics Approval and Consent to Participate

The Johns Hopkins University Institutional Review Board (#NA_00071337) approved all study procedures, and written informed consent was obtained from all participants.

Consent for Publication

All authors consent to the publication of this study.

Availability of Data and Material

The raw data supporting the conclusions of this manuscript will be made available by the authors without undue reservation.

Competing Interests

All authors declare that they have no competing interests.

Funding

This work was supported by grants from the National Institute on Aging (K00 AG068440-03 to KH, R00 AG062230 to GO, and R01 DC014475-05 and R01 AG068881-02 to KT) and grants from the National Institute of Biomedical Imaging and Bioengineering (R01 EB016089 to RE, and P41 EB031771).

Author Contributions

KH analyzed the MRS data, conducted all statistical analyses, created all figures and supplemental material, and wrote the first draft of the manuscript. HZ, GO, SH, AH, and RAE consulted on MRS data analyses and interpretation. HH contributed to manuscript writing and results interpretation. OH, JG, AH, and KT facilitated MRS and behavioral data collection. KT and RAE designed the project and led interpretation and discussion of the results. All authors participated in revision of the manuscript.

Acknowledgements

The authors also wish to thank all of the participants who volunteered their time, without whom this project would not have been possible.

518 **Abbreviations**

519 **PPA:** Primary progressive aphasia
520 **lvPPA:** logopenic variant PPA
521 **nfvPPA:** non-fluent variant PPA
522 **svPPA:** semantic variant PPA
523 **MRS:** magnetic resonance spectroscopy
524 **IFG:** inferior frontal gyrus
525 **SMC:** sensorimotor cortex
526 **tNAA:** total N-acetylaspartate
527 **tCho:** total choline
528 **tCr:** total creatine
529 **Glx:** glutamate+glutamine
530 **GABA:** gamma-aminobutyric acid
531 **AD:** Alzheimer's disease
532 **TE:** echo time
533 **PRESS:** Point RESolved Spectroscopy
534 **NAAG:** N-acetylaspartylglutamate
535 **PCh:** phosphocholine
536 **GPC:** glycerophosphocholine
537 **MEGA-PRESS:** MEscher–GArwood Point RESolved Spectroscopy
538 **MCI:** mild cognitive impairment
539 **tDCS:** transcranial direct current stimulation
540 **FTD-CDR:** FrontoTemporal Dementia Clinical Dementia Rating Scale
541 **MPRAGE:** magnetization-prepared rapid gradient-echo
542 **HSVD:** Hankel singular value decomposition
543 **MMs:** macromolecules
544 **Cr:** creatine
545 **PCr:** phosphocreatine
546 **ATP:** adenosine triphosphate
547 **ADP:** adenosine diphosphate
548 **AGAT:** glycine amidinotransferase
549 **GAMT:** guanidinoacetate methyltransferase
550 **SNPH:** syntaphilin
551

References

1. Gorno-Tempini ML, Hillis AE, Weintraub S, Kertesz A, Mendez M, Cappa SF, et al. Classification of primary progressive aphasia and its variants. Neurology. 2011;76(11):1006–14.

2. Mesulam M. Slowly progressive aphasia without generalized dementia. Ann Neurol Off J Am Neurol Assoc Child Neurol Soc. 1982;11(6):592–8.

3. Grossman M. Primary progressive aphasia: clinicopathological correlations. Nat Rev Neurol. 2010;6(2):88–97.

4. Hsiung GYR, Feldman HH. GRN frontotemporal dementia. GeneReviews. 2020;

5. Pagnoni I, Gobbi E, Premi E, Borroni B, Binetti G, Cotelli M, et al. Language training for oral and written naming impairment in primary progressive aphasia: A review. Transl Neurodegener. 2021;10(1):1–34.

6. Cotelli M, Manenti R, Ferrari C, Gobbi E, Macis A, Cappa SF. Effectiveness of language training and non-invasive brain stimulation on oral and written naming performance in Primary Progressive Aphasia: A meta-analysis and systematic review. Neurosci Biobehav Rev. 2020;108:498–525.

7. Tsapkini K, Webster KT, Ficek BN, Desmond JE, Onyike CU, Rapp B, et al. Electrical brain stimulation in different variants of primary progressive aphasia: A randomized clinical trial. Alzheimers Dement Transl Res Clin Interv. 2018;4:461–72.

8. Rogalski E, Cobia D, Martersteck A, Rademaker A, Wieneke C, Weintraub S, et al. Asymmetry of cortical decline in subtypes of primary progressive aphasia. Neurology. 2014;83(13):1184–91.

9. Mesulam M, Wicklund A, Johnson N, Rogalski E, Léger GC, Rademaker A, et al. Alzheimer and frontotemporal pathology in subsets of primary progressive aphasia. Ann Neurol Off J Am Neurol Assoc Child Neurol Soc. 2008;63(6):709–19.

10. Rabinovici GD, Jagust WJ, Furst AJ, Ogar JM, Racine CA, Mormino EC, et al. Aβ amyloid and glucose metabolism in three variants of primary progressive aphasia. Ann Neurol. 2008;64(4):388–401.

11. Josephs KA, Duffy JR, Strand EA, Whitwell JL, Layton KF, Parisi JE, et al. Clinicopathological and imaging correlates of progressive aphasia and apraxia of speech. Brain. 2006;129(6):1385–98.

12. Knibb JA, Xuereb JH, Patterson K, Hodges JR. Clinical and pathological characterization of progressive aphasia. Ann Neurol. 2006;59(1):156–65.

13. Davies RR, Hodges JR, Kril JJ, Patterson K, Halliday GM, Xuereb JH. The pathological basis of semantic dementia. Brain. 2005;128(9):1984–95.

14. Hodges JR, Davies RR, Xuereb JH, Casey B, Broe M, Bak TH, et al. Clinicopathological correlates in frontotemporal dementia. Ann Neurol. 2004;56(3):399–406.

589 15. Nestor PJ, Balan K, Cheow HK, Fryer TD, Knibb JA, Xuereb JH, et al. Nuclear imaging can
590 predict pathologic diagnosis in progressive nonfluent aphasia. Neurology. 2007;68(3):238–
591 9.

592 16. Bottomley P. Selective volume method for performing localized NMR spectroscopy.
593 US4480228A, 1982.

594 17. Rae CD. A guide to the metabolic pathways and function of metabolites observed in human
595 brain 1H magnetic resonance spectra. Neurochem Res. 2014;39(1):1–36.

596 18. Cleeland C, Pipingas A, Scholey A, White D. Neurochemical changes in the aging brain: A
597 systematic review. Neurosci Biobehav Rev. 2019;98:306–19.

598 19. Choi IY, Andronesi OC, Barker P, Bogner W, Edden RA, Kaiser LG, et al. Spectral editing in
599 1H magnetic resonance spectroscopy: Experts' consensus recommendations. NMR
600 Biomed. 2021;34(5):e4411.

601 20. Harris AD, Saleh MG, Edden RA. Edited 1H magnetic resonance spectroscopy in vivo:
602 Methods and metabolites. Magn Reson Med. 2017;77(4):1377–89.

603 21. Mescher M, Merkle H, Kirsch J, Garwood M, Gruetter R. Simultaneous in vivo spectral
604 editing and water suppression. NMR Biomed Int J Devoted Dev Appl Magn Reson Vivo.
605 1998;11(6):266–72.

606 22. Chiu PW, Mak HKF, Yau KKW, Chan Q, Chang RCC, Chu LW. Metabolic changes in the
607 anterior and posterior cingulate cortices of the normal aging brain: proton magnetic
608 resonance spectroscopy study at 3 T. Age. 2014;36(1):251–64.

609 23. Gao F, Edden RA, Li M, Puts NA, Wang G, Liu C, et al. Edited magnetic resonance
610 spectroscopy detects an age-related decline in brain GABA levels. Neuroimage.
611 2013;78:75–82.

612 24. Haga KK, Khor YP, Farrall A, Wardlaw JM. A systematic review of brain metabolite
613 changes, measured with 1H magnetic resonance spectroscopy, in healthy aging. Neurobiol
614 Aging. 2009;30(3):353–63.

615 25. Oeltzschner G, Wijtenburg SA, Mikkelsen M, Edden RA, Barker PB, Joo JH, et al.
616 Neurometabolites and associations with cognitive deficits in mild cognitive impairment: a
617 magnetic resonance spectroscopy study at 7 Tesla. Neurobiol Aging. 2019;73:211–8.

618 26. Zeydan B, Deelchand DK, Tosakulwong N, Lesnick TG, Kantarci OH, Machulda MM, et al.
619 Decreased glutamate levels in patients with amnestic mild cognitive impairment: An
620 sLASER proton MR spectroscopy and PiB-PET study. J Neuroimaging. 2017;27(6):630–6.

621 27. Bai X, Edden RA, Gao F, Wang G, Wu L, Zhao B, et al. Decreased γ-aminobutyric acid
622 levels in the parietal region of patients with Alzheimer's disease. J Magn Reson Imaging.
623 2015;41(5):1326–31.

624 28. Rupsingh R, Borrie M, Smith M, Wells JL, Bartha R. Reduced hippocampal glutamate in
625 Alzheimer disease. Neurobiol Aging. 2011;32(5):802–10.

29. Wang H, Tan L, Wang HF, Liu Y, Yin RH, Wang WY, et al. Magnetic resonance spectroscopy in Alzheimer's disease: systematic review and meta-analysis. J Alzheimers Dis. 2015;46(4):1049–70.

30. Zhang N, Song X, Bartha R, Beyea S, D'Arcy R, Zhang Y, et al. Advances in high-field magnetic resonance spectroscopy in Alzheimer's disease. Curr Alzheimer Res. 2014;11(4):367–88.

31. Huang W, Alexander GE, Chang L, Shetty HU, Krasuski JS, Rapoport SI, et al. Brain metabolite concentration and dementia severity in Alzheimer's disease: a 1H MRS study. Neurology. 2001;57(4):626–32.

32. Marjańska M, McCarten JR, Hodges JS, Hemmy LS, Terpstra M. Distinctive neurochemistry in Alzheimer's Disease via 7 T in vivo magnetic resonance spectroscopy. J Alzheimers Dis. 2019;68(2):559–69.

33. Erickson KI, Weinstein AM, Sutton BP, Prakash RS, Voss MW, Chaddock L, et al. Beyond vascularization: aerobic fitness is associated with N-acetylaspartate and working memory. Brain Behav. 2012;2(1):32–41.

34. Gomar JJ, Gordon ML, Dickinson D, Kingsley PB, Uluğ AM, Keehlisen L, et al. APOE genotype modulates proton magnetic resonance spectroscopy metabolites in the aging brain. Biol Psychiatry. 2014;75(9):686–92.

35. Kantarci K, Lowe V, Przybelski SA, Senjem ML, Weigand SD, Ivnik RJ, et al. Magnetic resonance spectroscopy, β-amyloid load, and cognition in a population-based sample of cognitively normal older adults. Neurology. 2011;77(10):951–8.

36. Porges EC, Woods AJ, Edden RA, Puts NA, Harris AD, Chen H, et al. Frontal gamma-aminobutyric acid concentrations are associated with cognitive performance in older adults. Biol Psychiatry Cogn Neurosci Neuroimaging. 2017;2(1):38–44.

37. Ross AJ, Sachdev PS, Wen W, Valenzuela MJ, Brodaty H. Cognitive correlates of 1H MRS measures in the healthy elderly brain. Brain Res Bull. 2005;66(1):9–16.

38. Griffith HR, den Hollander JA, Okonkwo O, Evanochko WT, Harrell LE, Zamrini EY, et al. Executive function is associated with brain proton magnetic resonance spectroscopy in amnestic mild cognitive impairment. J Clin Exp Neuropsychol. 2007;29(6):599–609.

39. Lim TS, Hong YH, Choi JY, Kim HS, Moon SY. Functional investigation of bilateral posterior cingulate gyri using multivoxel MR spectroscopy. Eur Neurol. 2012;67(5):279–86.

40. Riese F, Gietl A, Zölch N, Henning A, O'Gorman R, Kälin AM, et al. Posterior cingulate γ-aminobutyric acid and glutamate/glutamine are reduced in amnestic mild cognitive impairment and are unrelated to amyloid deposition and apolipoprotein E genotype. Neurobiol Aging. 2015;36(1):53–9.

41. Murley AG, Tsvetanov KA, Rouse MA, Jones PS, Sværke K, Li W, et al. Proton magnetic resonance spectroscopy in frontotemporal lobar degeneration-related syndromes. Neurobiol Aging. 2022;111:64–70.

42. Harris AD, Wang Z, Ficek B, Webster K, Edden RA, Tsapkini K. Reductions in GABA following a tDCS-language intervention for primary progressive aphasia. Neurobiol Aging. 2019;79:75–82.

43. Knopman DS, Kramer JH, Boeve BF, Caselli RJ, Graff-Radford NR, Mendez MF, et al. Development of methodology for conducting clinical trials in frontotemporal lobar degeneration. Brain. 2008;131(11):2957–68.

44. Tkáč I, Starčuk Z, Choi IY, Gruetter R. In vivo 1H NMR spectroscopy of rat brain at 1 ms echo time. Magn Reson Med Off J Int Soc Magn Reson Med. 1999;41(4):649–56.

45. Harris AD, Puts NA, Barker PB, Edden RA. Spectral-editing measurements of GABA in the human brain with and without macromolecule suppression. Magn Reson Med. 2015;74(6):1523–9.

46. Oeltzschner G, Zöllner HJ, Hui SC, Mikkelsen M, Saleh MG, Tapper S, et al. Osprey: Open-source processing, reconstruction & estimation of magnetic resonance spectroscopy data. J Neurosci Methods. 2020;343:108827.

47. Wilson M, Andronesi O, Barker PB, Bartha R, Bizzi A, Bolan PJ, et al. Methodological consensus on clinical proton MRS of the brain: Review and recommendations. Magn Reson Med. 2019;82(2):527–50.

48. Zöllner HJ, Považan M, Hui SC, Tapper S, Edden RA, Oeltzschner G. Comparison of different linear-combination modeling algorithms for short-TE proton spectra. NMR Biomed. 2021;34(4):e4482.

49. Zöllner HJ, Tapper S, Hui SC, Barker PB, Edden RA, Oeltzschner G. Comparison of linear combination modeling strategies for edited magnetic resonance spectroscopy at 3 T. NMR Biomed. 2022;35(1):e4618.

50. Barkhuijsen H, De Beer R, Van Ormondt D. Improved algorithm for noniterative time-domain model fitting to exponentially damped magnetic resonance signals. J Magn Reson 1969. 1987;73(3):553–7.

51. Hui SC, Saleh M, Zoellner HJ, Oeltzschner G, Fan H, Li Y, et al. MRSCloud: a Cloud-based MR Spectroscopy Tool for Basis Set Simulation. bioRxiv. 2022;

52. Ashburner J, Barnes G, Chen CC, Daunizeau J, Flandin G, Friston K, et al. SPM12 manual. Wellcome Trust Cent Neuroimaging Lond UK. 2014;2464:4.

53. Klose U. In vivo proton spectroscopy in presence of eddy currents. Magn Reson Med. 1990;14(1):26–30.

54. Mikkelsen M, Tapper S, Near J, Mostofsky SH, Puts NA, Edden RA. Correcting frequency and phase offsets in MRS data using robust spectral registration. NMR Biomed. 2020;33(10):e4368.

55. Deelchand DK, Marjańska M, Henry PG, Terpstra M. MEGA-PRESS of GABA+: influences of acquisition parameters. NMR Biomed. 2021;34(5):e4199.

701 56. Porges EC, Woods AJ, Lamb DG, Williamson JB, Cohen RA, Edden RA, et al. Impact of
702 tissue correction strategy on GABA-edited MRS findings. Neuroimage. 2017;162:249–56.

703 57. Wansapura JP, Holland SK, Dunn RS, Ball Jr WS. NMR relaxation times in the human brain
704 at 3.0 tesla. J Magn Reson Imaging Off J Int Soc Magn Reson Med. 1999;9(4):531–8.

705 58. Gasparovic C, Song T, Devier D, Bockholt HJ, Caprihan A, Mullins PG, et al. Use of tissue
706 water as a concentration reference for proton spectroscopic imaging. Magn Reson Med Off
707 J Int Soc Magn Reson Med. 2006;55(6):1219–26.

708 59. Harris AD, Puts NA, Edden RA. Tissue correction for GABA-edited MRS: Considerations of
709 voxel composition, tissue segmentation, and tissue relaxations. J Magn Reson Imaging.
710 2015;42(5):1431–40.

711 60. Lin A, Andronesi O, Bogner W, Choi IY, Coello E, Cudalbu C, et al. Minimum reporting
712 standards for in vivo magnetic resonance spectroscopy (MRSinMRS): experts' consensus
713 recommendations. NMR Biomed. 2021;34(5):e4484.

714 61. R Core Team. R: A language and environment for statistical computing. [Internet]. Vienna,
715 Austria: R Foundation for Statistical Computing; 2021. Available from: https://www.R-
716 project.org/

717 62. RStudio Team. RStudio: Integrated Development Environment for R [Internet]. Boston, MA:
718 RStudio, PBC; 2021. Available from: http://www.rstudio.com/

719 63. Pinheiro JC, Bates DM. Theory and computational methods for linear mixed-effects models.
720 Mix-Eff Models -PLUS. 2000;57–96.

721 64. Hupfeld KE, Hyatt HW, Alvarez Jerez P, Mikkelsen M, Hass CJ, Edden RAE, et al. In vivo
722 brain glutathione is higher in older age and correlates with mobility. Cereb Cortex.
723 2021;31(10):4576–94.

724 65. McLeod AI, Xu C. bestglm: Best subset GLM. URL HttpCRAN R-Proj Orgpackage Bestglm.
725 2010;

726 66. Zhang Z. Variable selection with stepwise and best subset approaches. Ann Transl Med.
727 2016;4(7).

728 67. Bürklen TS, Schlattner U, Homayouni R, Gough K, Rak M, Szeghalmi A, et al. The creatine
729 kinase/creatine connection to alzheimer's disease: CK Inactivation, APP-CK complexes
730 and focal creatine deposits. J Biomed Biotechnol. 2006;2006.

731 68. Rackayova V, Cudalbu C, Pouwels PJ, Braissant O. Creatine in the central nervous system:
732 From magnetic resonance spectroscopy to creatine deficiencies. Anal Biochem.
733 2017;529:144–57.

734 69. Reyngoudt H, Claeys T, Vlerick L, Verleden S, Acou M, Deblaere K, et al. Age-related
735 differences in metabolites in the posterior cingulate cortex and hippocampus of normal
736 ageing brain: a 1H-MRS study. Eur J Radiol. 2012;81(3):e223–31.

70. Charlton RA, McIntyre DJO, Howe FA, Morris RG, Markus HS. The relationship between white matter brain metabolites and cognition in normal aging: the GENIE study. Brain Res. 2007;1164:108–16.

71. Chang L, Ernst T, Poland RE, Jenden DJ. In vivo proton magnetic resonance spectroscopy of the normal aging human brain. Life Sci. 1996;58(22):2049–56.

72. Pfefferbaum A, Adalsteinsson E, Spielman D, Sullivan EV, Lim KO. In vivo spectroscopic quantification of the N-acetyl moiety, creatine, and choline from large volumes of brain gray and white matter: Effects of normal aging. Magn Reson Med Off J Int Soc Magn Reson Med. 1999;41(2):276–84.

73. Chang L, Ernst T, Witt MD, Ames N, Gaiefsky M, Miller E. Relationships among brain metabolites, cognitive function, and viral loads in antiretroviral-naıve HIV patients. Neuroimage. 2002;17(3):1638–48.

74. Chang L, Ernst T, Witt MD, Ames N, Walot I, Jovicich J, et al. Persistent brain abnormalities in antiretroviral-naive HIV patients 3 months after HAART. Antivir Ther. 2003;8(1):17–26.

75. Smith CD, Landrum W, Carney JM, Landfield PW, Avison MJ. Brain creatine kinase with aging in F-344 rats: analysis by saturation transfer magnetic resonance spectroscopy. Neurobiol Aging. 1997;18(6):617–22.

76. Pettegrew JW, Panchalingam K, Klunk WE, McClure RJ, Muenz LR. Alterations of cerebral metabolism in probable Alzheimer's disease: a preliminary study. Neurobiol Aging. 1994;15(1):117–32.

77. McIntyre DJ, Charlton RA, Markus HS, Howe FA. Long and short echo time proton magnetic resonance spectroscopic imaging of the healthy aging brain. J Magn Reson Imaging Off J Int Soc Magn Reson Med. 2007;26(6):1596–606.

78. Adhihetty PJ, Beal MF. Creatine and its potential therapeutic value for targeting cellular energy impairment in neurodegenerative diseases. Neuromolecular Med. 2008;10(4):275–90.

79. Oeltzschner G, Saleh MG, Rimbault D, Mikkelsen M, Chan KL, Puts NA, et al. Advanced Hadamard-encoded editing of seven low-concentration brain metabolites: Principles of HERCULES. Neuroimage. 2019;185:181–90.

80. Cheng XT, Sheng ZH. Developmental regulation of microtubule-based trafficking and anchoring of axonal mitochondria in health and diseases. Dev Neurobiol. 2021;81(3):284–99.

81. Kang JS, Tian JH, Pan PY, Zald P, Li C, Deng C, et al. Docking of axonal mitochondria by syntaphilin controls their mobility and affects short-term facilitation. Cell. 2008;132(1):137–48.

82. Andres-Benito P, Gelpi E, Povedano M, Ausin K, Fernandez-Irigoyen J, Santamaría E, et al. Combined transcriptomics and proteomics in frontal cortex area 8 in frontotemporal lobar degeneration linked to C9orf72 expansion. J Alzheimers Dis. 2019;68(3):1287–307.

775 83. Fukumitsu K, Fujishima K, Yoshimura A, Wu YK, Heuser J, Kengaku M. Synergistic action
776 of dendritic mitochondria and creatine kinase maintains ATP homeostasis and actin
777 dynamics in growing neuronal dendrites. J Neurosci. 2015;35(14):5707–23.

778 84. Morsci NS, Hall DH, Driscoll M, Sheng ZH. Age-related phasic patterns of mitochondrial
779 maintenance in adult Caenorhabditis elegans neurons. J Neurosci. 2016;36(4):1373–85.

780 85. Vagnoni A, Bullock SL. A cAMP/PKA/Kinesin-1 axis promotes the axonal transport of
781 mitochondria in aging Drosophila neurons. Curr Biol. 2018;28(8):1265-1272. e4.

782 86. Saunders DE, Howe FA, van den Boogaart A, Griffiths JR, Brown MM. Aging of the adult
783 human brain: in vivo quantitation of metabolite content with proton magnetic resonance
784 spectroscopy. J Magn Reson Imaging Off J Int Soc Magn Reson Med. 1999;9(5):711–6.

785 87. Ratai EM, Annamalai L, Burdo T, Joo CG, Bombardier JP, Fell R, et al. Brain creatine
786 elevation and N-acetylaspartate reduction indicates neuronal dysfunction in the setting of
787 enhanced glial energy metabolism in a macaque model of NeuroAIDS. Magn Reson Med.
788 2011;66(3):625–34.

789 88. Urenjak J, Williams SR, Gadian DG, Noble M. Proton nuclear magnetic resonance
790 spectroscopy unambiguously identifies different neural cell types. J Neurosci.
791 1993;13(3):981–9.

792 89. Kim G, Ahmadian SS, Peterson M, Parton Z, Memon R, Weintraub S, et al. Asymmetric
793 pathology in primary progressive aphasia with progranulin mutations and TDP inclusions.
794 Neurology. 2016;86(7):627–36.

795 90. Ohm DT, Kim G, Gefen T, Rademaker A, Weintraub S, Bigio EH, et al. Prominent microglial
796 activation in cortical white matter is selectively associated with cortical atrophy in primary
797 progressive aphasia. Neuropathol Appl Neurobiol. 2019;45(3):216–29.

798 91. Mosser DM, Edwards JP. Exploring the full spectrum of macrophage activation. Nat Rev
799 Immunol. 2008;8(12):958–69.

800 92. Perry VH, Nicoll JA, Holmes C. Microglia in neurodegenerative disease. Nat Rev Neurol.
801 2010;6(4):193–201.

802 93. Rosen HJ, Allison SC, Ogar JM, Amici S, Rose K, Dronkers N, et al. Behavioral features in
803 semantic dementia vs other forms of progressive aphasias. Neurology. 2006;67(10):1752–
804 6.

805 94. Gomez-Tortosa E, Rigual R, Prieto-Jurczynska C, Mahillo-Fernandez I, Guerrero-Lopez R,
806 Perez-Perez J, et al. Behavioral evolution of progressive semantic aphasia in comparison
807 with nonfluent aphasia. Dement Geriatr Cogn Disord. 2016;41(1–2):1–8.

808 95. Liakakis G, Nickel J, Seitz R. Diversity of the inferior frontal gyrus—a meta-analysis of
809 neuroimaging studies. Behav Brain Res. 2011;225(1):341–7.

810 96. Avgerinos KI, Spyrou N, Bougioukas KI, Kapogiannis D. Effects of creatine supplementation
811 on cognitive function of healthy individuals: A systematic review of randomized controlled
812 trials. Exp Gerontol. 2018;108:166–73.

813 97. Levin O, Weerasekera A, King BR, Heise KF, Sima DM, Chalavi S, et al. Sensorimotor
814 cortex neurometabolite levels as correlate of motor performance in normal aging: evidence
815 from a 1H-MRS study. NeuroImage. 2019;202:116050.

816 98. Zahr NM, Mayer D, Rohlfing T, Chanraud S, Gu M, Sullivan EV, et al. In vivo glutamate
817 measured with magnetic resonance spectroscopy: behavioral correlates in aging.
818 Neurobiol Aging. 2013;34(4):1265–76.

819 99. Murley AG, Rouse MA, Jones PS, Ye R, Hezemans FH, O'Callaghan C, et al. GABA and
820 glutamate deficits from frontotemporal lobar degeneration are associated with disinhibition.
821 Brain. 2020;143(11):3449–62.

822 100. Duffy SL, Lagopoulos J, Hickie IB, Diamond K, Graeber MB, Lewis SJ, et al. Glutathione
823 relates to neuropsychological functioning in mild cognitive impairment. Alzheimers Dement.
824 2014;10(1):67–75.

825 101. Deelchand DK, McCarten JR, Hemmy LS, Auerbach EJ, Eberly LE, Marjańska M.
826 Changes in the intracellular microenvironment in the aging human brain. Neurobiol Aging.
827 2020;95:168–75.

828 102. Marjańska M, Emir UE, Deelchand DK, Terpstra M. Faster metabolite 1H transverse
829 relaxation in the elder human brain. PloS One. 2013;8(10):e77572.

830 103. Marjańska M, McCarten JR, Hodges J, Hemmy LS, Grant A, Deelchand DK, et al. Region-
831 specific aging of the human brain as evidenced by neurochemical profiles measured
832 noninvasively in the posterior cingulate cortex and the occipital lobe using 1H magnetic
833 resonance spectroscopy at 7 T. Neuroscience. 2017;354:168–77.

834